Electronic and structural properties of the honeycomb iridates A_2IrO_3 (A = Na, Li) at elevated pressures

Samar Layek ☉,[1,2,3,*] Kavita Mehlawat,[4] D. Levy,[1] E. Greenberg,[1,5] M. P. Pasternak,[1] Jean-Paul Itié,[6]
Yogesh Singh,[4] and G. Kh. Rozenberg[1]

[1]*School of Physics and Astronomy, Tel Aviv University, 69978 Tel Aviv, Israel*
[2]*Cavendish Laboratory, Department of Physics, University of Cambridge, Cambridge CB3 0HE, United Kingdom*
[3]*CNRS, Université Grenoble Alpes, Institut Néel, 38042 Grenoble, France*
[4]*Department of Physical Sciences, Indian Institute of Science Education and Research (IISER) Mohali,
Knowledge City, Sector 81, Mohali 140306, India*
[5]*GSECARS, University of Chicago, Chicago, Illinois 60637, USA*
[6]*Synchrotron SOLEIL, L'Orme des Merisiers, Saint-Aubin, BP 48, 91192 Gif-sur-Yvette Cedex, France*

The honeycomb lattice iridates A_2IrO_3 (A = Na, Li) are spin-orbit assisted Mott insulators proximate to Kitaev's quantum spin liquid. The insulating state as well as the magnetic properties are believed to arise due to a delicate balance of several energy scales. We report on high-pressure electrical transport and x-ray-diffraction measurements on A_2IrO_3 (A = Na, Li) in an attempt to study their structural and electronic evolution with pressure. We found that while Li_2IrO_3 undergoes a structural phase transition into the dimerized state at a pressure of $P \sim 4$ GPa, in Na_2IrO_3 the conservation of the original $C2/m$ structure up to at least 58 GPa is observed. In addition, Li_2IrO_3 undergoes a sluggish structural rearrangement at the pressure range 20–40 GPa coinciding with a significant decrease in resistance. Despite dissimilar structural evolution and different mechanisms of the electrical conductivity, Arrhenius conductivity for Na_2IrO_3 and Mott variable-range hopping in Li_2IrO_3, both systems show a very similar $R(P)$ behavior. Namely, after a nonmonotonic decrease of the resistance R and the charge gap Δ, the Δ stabilizes at about 45 GPa and even increases slightly with pressure; the $R(T)$ shows insulating behavior up to the highest pressure measured, 80 and 55 GPa, respectively. This resilient nonmetallic behavior of the studied iridates suggests a formation close to a localized-itinerant crossover of unusual electronic states, whose possible features are discussed. Unforeseeably, the $R(P)$ behavior is not dependent on the buffer element A, which seems essential for understanding the nature of the electrical conductivity in iridates.

I. INTRODUCTION

The quasi-two-dimensional (2D) honeycomb lattice iridates A_2IrO_3 (A = Na, Li) have been studied extensively as possible materials hosting Kitaev-like interactions [1–17]. The Mott insulating state in these materials arises from a delicate balance between spin-orbit coupling and electronic correlations, both of which need to be put on an equal footing. In addition, other energy scales like octahedral distortions, Hund's coupling, etc., may become important when structural distortions are present [18]. This has led to the study of a variety of low-energy Hamiltonians to try to understand the electronic and magnetic properties of these iridates [18]. In addition, this family of honeycomb lattice materials also seems susceptible to structural dimerization instabilities as have been observed for Li_2RuO_3 [19,20], α-$RuCl_3$ [21,22], and more recently α-Li_2IrO_3 [23–25].

It is noteworthy that in iridates a metallic ground state could be expected, due to the highly delocalized $5d$ elec-

tronic orbitals of the Ir ions. However, nonmetallic behavior has been found in many iridates [26]. The unexpected insulating behavior has been attributed to the strong spin-orbit coupling (SOC), comparable, as it was mentioned above, to the Coulomb repulsion, giving rise to an unusual $J_{eff} = 1/2$ Mott-insulating ground state [27–29]. Thus, in Ir-based pyrochlores for weak electron-electron interactions Ir electrons are in metallic and topological band insulator phases at weak and strong spin-orbit interactions, respectively [30]. The interaction features could be modified by a chemical substitution or external pressure: hydrostatic pressure is a particularly effective tuning parameter, as it can be used to directly modify the overlap between electronic orbitals, and thereby control the electron interactions. A usual result of the pressure application is a closure of an insulating gap and an insulator-metal transition due to an appreciable unit-cell volume densification and corresponding bandwidth broadening. However, recent studies of Sr_2IrO_4 and $Sr_3Ir_2O_7$, characterized by the rather small ambient pressure energy gap of $\sim$0.25 eV, demonstrate a remarkable persistence of the nonmetallic state up to the maximum pressures achieved, 55 and 104 GPa, respectively [31]. (Interestingly, single-crystal $Sr_3Ir_2O_7$

*Corresponding author: samarlayek@gmail.com

resistance measurements above 59 GPa show metallicity in the *ab* plane but an insulating behavior along the *c* axis [32].) Furthermore, a very recent study of Sr_2IrO_4 showed that a stable insulating state persists even up to 185 GPa [33]. Such a behavior is rather unusual and needs further investigation.

Along with the strength of spin-orbit coupling, the strength of correlation effects and Hund's rule coupling, one of the factors which controls the competition between Kitaev physics, magnetism, and dimerization in A_2MO_3 honeycomb networks is the ionic radii of the buffer element A. In this context it is particularly instructive to compare α-Li_2IrO_3 with Na_2IrO_3, whose buffer elements have very different ionic radii, and furthermore, to compare the obtained data with the results for Sr iridates [31–33]. In this work we report a combined powder x-ray diffraction (XRD) and electrical transport studies of the structural and electronic properties of A_2IrO_3 (A = Na, Li) at pressures up to 80 GPa. We show that despite different buffer elements and correspondingly a rather different structural behavior and diverse conductivity mechanism, both systems demonstrate very similar $R(P)$ features. Furthermore, at about 45 GPa the charge gap Δ stabilizes in both systems and stays finite, and the electrical resistance $R(T)$ shows insulating behavior up to the highest pressure measured. This resilient nonmetallic behavior of the iridates, despite a significant unit-cell volume decrease, is of great interest and suggests the formation of unusual electronic states, close to a localized-itinerant crossover [5,34].

II. EXPERIMENT

Polycrystalline samples of A_2IrO_3 were synthesized using a solid-state reaction method starting with high purity chemicals and heating the pelletized mixtures between 900 and 1000 °C in 50° steps. The stepwise heating instead of going directly to 1000 °C was found to be essential for the formation of high quality samples. Powder x-ray diffraction on crushed pieces of the samples confirmed the formation of single phase samples with lattice parameters consistent with previous reports [8].

Powder XRD measurements at high pressures were carried out at room temperature in angle-dispersive mode with a wavelength of $\lambda = 0.3738$ Å at the Pression Structure Imagerie par Contraste à Haute Énergie (PSICHÉ) beamline of Synchrotron Soleil (Paris). Pressurization was by means of a miniature TAU piston-cylinder diamond-anvil cell (DAC) [35] with anvils having 300-μm diameter culets. The sample, along with a few ruby chips, was loaded into a 100-μm-diameter cavity drilled in a rhenium gasket preindented down to a final thickness of $\sim$15 μm. Ar_2 and N_2 were used as the pressure-transmitting medium. Diffraction images were collected using a MAR345 image plate detector and integrated using the FIT2D [36,37] and DIOPTAS software [38]. Diffraction patterns were analyzed using the GSAS-II software [39] to extract the unit-cell parameters.

The intensities of the diffraction peaks are affected by instrumental and grain-size issues (diamond x-ray absorption and low statistics in random distribution of the sample crystallites). Therefore, the Rietveld refinement of the powder-diffraction patterns did not result in a good enough fit. Hence, diffraction patterns were analyzed by using the whole profile fitting (Pawley) method [40]. In the case of Na_2IrO_3 diffraction spectra mainly exhibit peaks from the sample, as well as minor peak contributions from an IrO_2 impurity. This phase was considered in the refinements. The reliability factor R_{wp} obtained in the refinement of each of the powder diffraction patterns is $\sim$5%.

Additional sets of XRD measurements were performed for Na_2IrO_3 and Li_2IrO_3 at extended pressure ranges up to 58 and 71 GPa at the beamlines 13-BM-C and 13-ID-D of APS (Argonne, IL, USA), with wavelengths of $\lambda = 0.434$ and 0.3344 Å, respectively, in angle-dispersive mode with patterns collected using a Pilatus 1M Si and Pilatus 1M CdTe detector, respectively. Ne was used as the pressure-transmitting medium in this measurement. It also served as a pressure marker. Ruby was used as a pressure gauge as well.

Electrical transport measurements up to $P \approx 3$ GPa were made using a high-pressure cell in a Quantum Design physical property measurement system (QD-PPMS). Higher pressure transport measurements up to $P \sim 80$ GPa were performed using a TAU piston-cylinder DAC with anvils having culets of diameter 220 μm. Pressed powder samples were loaded into 100-μm-diameter cavities drilled in a rhenium gasket insulated with a layer of Al_2O_3-NaCl (3:1 atomic ratio) mixed with epoxy, which also serves as the pressure medium. Six platinum triangles, serving as electrodes, were placed on the culet to permit measurements in various DC four-probe arrangements at a given pressure. The Pt electrodes were connected to exterior conducting wires by a silver epoxy. Resistance was measured as a function of pressure and temperature (for both compression and decompression cycles) using a standard four-probe method in a custom-made cryostat. At each temperature, the voltage was measured as a function of a series of applied currents, for determining the resistance from the obtained slope. The temperature was measured using a Lakeshore Si (DT-421-HR) diode in proximity to the DAC.

A few ruby fragments were placed in the center region of the culet between the Pt electrodes overlapping the sample for pressure calibration. Pressure was measured both before and after each measurement from the ruby fluorescence spectra using the calibration scales mentioned in Ref. [41]. Raman spectra from the diamond anvils were also used to determine the pressure, especially at pressures higher than 60 GPa [42]. Pressure gradients were measured to be small ($\sim$5%) in the distances 15–20 μm between the tips of the Pt electrodes across which voltage was measured.

III. RESULTS

A. X-ray-diffraction study

1. Li₂IrO₃

Figures 1(a) and 1(b) show the powder x-ray-diffraction pattern for Li_2IrO_3 for various pressures $P \leqslant 31.5$ and 71 GPa obtained at Soleil and APS synchrotron facilities, respectively. Up to $P = 3.3$ GPa, the XRD pattern matches the ambient pressure structure. A first-order structural transition occurs above $P = 3.3$ GPa. At 4.3 and 5.7 GPa (not shown) the main diffraction lines already belong to a new high-pressure (HP) phase but traces of the low-pressure (LP) phase could be distinguished. For $P \geqslant 7.7$ GPa, only the HP phase exists.
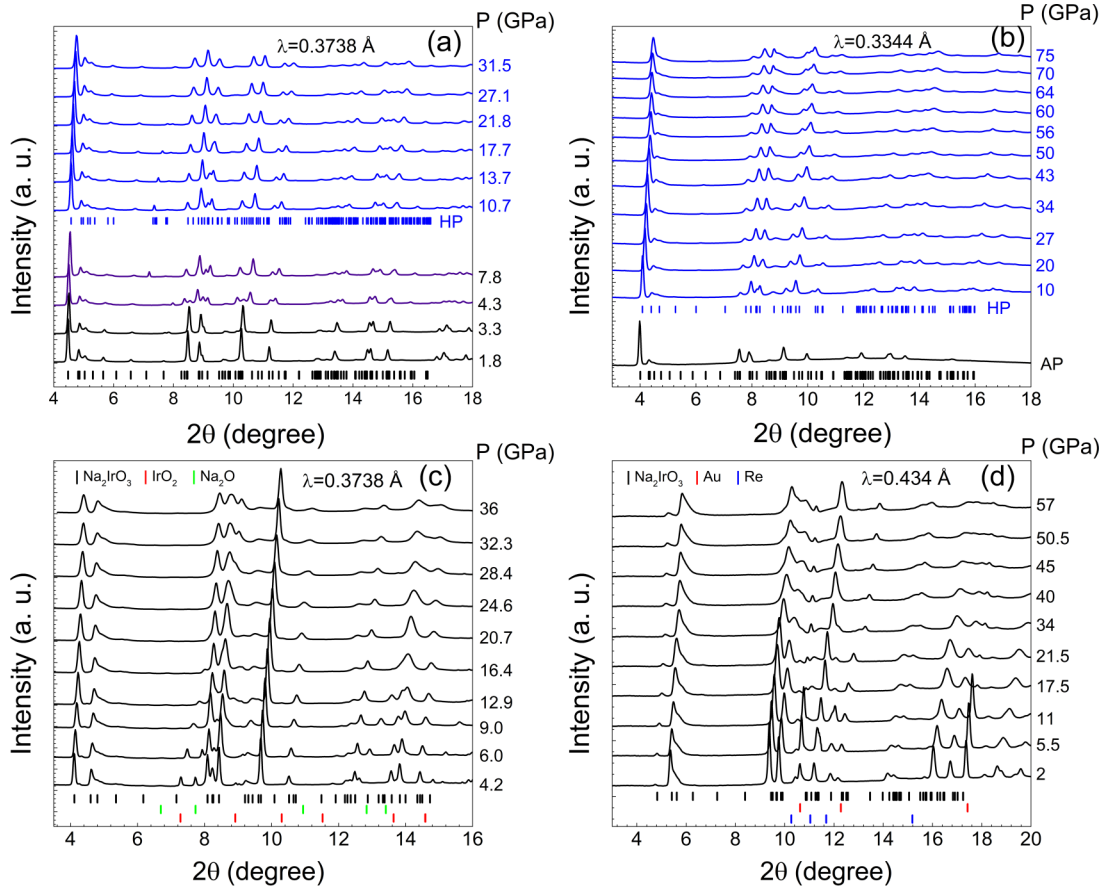
FIG. 1. Powder x-ray-diffraction patterns for Li_2IrO_3 (a), (b) and Na_2IrO_3 (c), (d) at various pressures obtained at Soleil (a), (c) and APS (b), (d). For (c) and (d) the intensity ratio of peaks is rather different, presumably due to the effect of different preferential orientations for different sample batches and loadings. Note the first-order structural phase transition above $P = 3.3$ GPa in Li_2IrO_3.

Diffraction patterns up to 3.3 GPa may be refined in terms of a monoclinic ($C2/m$, no. 12) structure [see Fig. 2(a)], while the structural transition involves a symmetry reduction to triclinic (P-1) phase [Fig. 2(b)]. These results are consistent with recent high-pressure x-ray studies on single crystals [24] and powders (see Ref. [25] and references therein) of Li_2IrO_3. In the high-pressure structure according to [23–25], Ir-Ir structural dimerization takes place.

The pressure dependence of the lattice parameters and crystal volume for Li_2IrO_3 is illustrated in Fig. 3 (we used $b' = b/\sqrt{3}$ for a better comparison between the three lattice parameters). These parameters reveal (i) a sharp, discontinuous change in unit-cell lengths, unit-cell angles, and crystal volume above 3.3 GPa resulting from a crystal symmetry change, (ii) the conservation of the HP triclinic P-1 structure at least up to ∼71 GPa [Fig. 1(b)] with an appreciable change of the a-parameter behavior and a tiny change of the crystal volume features above 20 GPa. Solid lines through the data symbols are fits with a Birch-Murnaghan equation of state (EOS) to obtain bulk modulus K_0, its pressure derivative K_0', and unit-cell volume V_0 [43]. The obtained values of K_0 and the V_0 at 1 bar and 300 K are in reasonable agreement with the single-crystal data [24]. We note that around 20 GPa compressibility of the a axis strongly decreases (∼3 times) and it shows the high stiffness between 20 and about 40 GPa

followed by a steeper decrease with pressure increase above ∼40 GPa coinciding with a steeper decrease of the c parameter at the 40–50-GPa range. $V(P)$ data show some deviation from the calculated EOS between about 28 and 40 GP; the monoclinic angle β increases slightly around 45 GPa. Such parameter behavior suggests a possible structural realignment, taking place mainly in the a-b' plane at the 20–40-GPa range within the same HP structure. Indeed, the b'/a ratio, representing the degree of the honeycomb lattice distortion due to Ir-Ir dimerization, which increases strongly as the result of dimerization around 4 GPa and hardly changes up to 20 GPa, shows an appreciable decrease between 20 and 40 GPa followed by stabilization above 40 GPa [see inset Fig. 3(a)].

2. Na_2IrO_3

Figures 1(c) and 1(d) show the powder x-ray-diffraction pattern for Na_2IrO_3 for various pressures $P \leqslant 36$ and 58 GPa obtained at Soleil and APS synchrotron facilities, respectively. Diffraction patterns within the whole pressure range may be refined in terms of a monoclinic ($C2/m$) structure [see Figs. 2(d)–2(f)]. These results are consistent with recent high-pressure single-crystal x-ray studies [44] of Na_2IrO_3 performed up to 25 GPa. The pressure dependence of the lattice parameters and crystal volume for Na_2IrO_3 is illustrated in
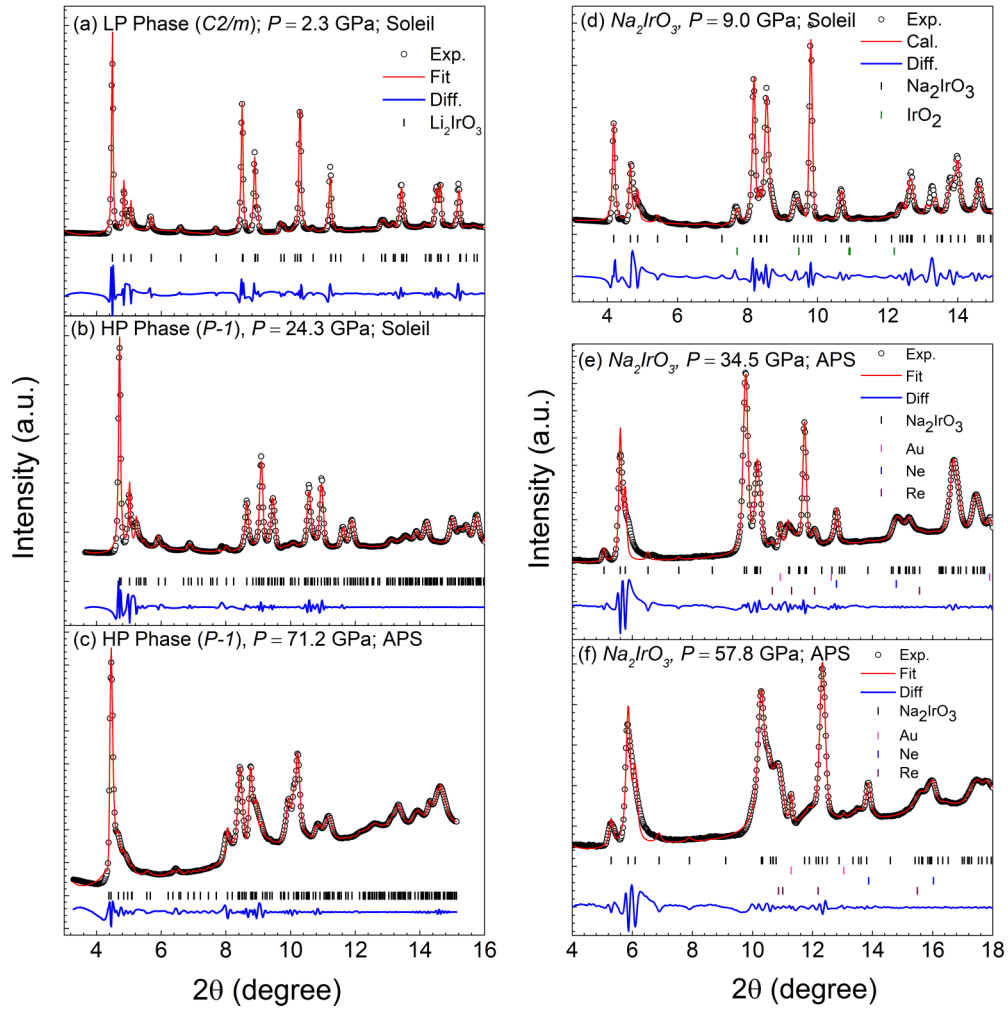
FIG. 2. Refinement of XRD patterns collected at $T = 300$ K for Li_2IrO_3 (a)–(c) and for Na_2IrO_3 (d)–(f) at 2.3, 24.3, 71.2, 9, 34.5, and 57.8 GPa, respectively and the differences between the observed and calculated profiles. Marks show the calculated peak positions. The 2.3-GPa pattern corresponds to the LP phase of Li_2IrO_3 with $C2/m$ symmetry, extending from ambient pressure to $\sim$4 GPa. Above $\sim$4 GPa the symmetry group is P-1. Contamination reflections from minor phase IrO_2 remnant, Au pressure marker, Re gasket, and Ne are indicated in the case of Na_2IrO_3.

Fig. 4 The data for both sets of measurements are consistent: the lattice parameters and crystal volume reveal a monotonic decrease within the studied pressure range with relatively easy compression along the c axis; the β angle increases slowly. The solid line through the data symbols is the fit with a second-order Birch-Murnaghan EOS. The obtained value of bulk modulus 108(1) GPa is in reasonable agreement with the single-crystal data [43].

B. Electrical transport measurements

1. Li₂IrO₃

Figure 5(a) shows the variation of the resistance R versus pressure at $T = 300$ K for Li_2IrO_3. Measurements were performed with three different configurations of voltage contacts, all showing very similar behavior. Correspondingly, on the plot we report mean values for three different contact combinations. It is observed that initially, R decreases gradually with increasing pressure up to about 12 GPa. In particular, there is

no abrupt change in R across the first-order structural change between 3.3 and 6 GPa. Above 12 GPa, a much more rapid decrease in R occurs on increasing pressure up to about 22 GPa. After this R again gradually decreases with P until about 44 GPa. Beyond $P \sim 45$ GPa, the resistance hardly changes with pressure. The decrease in resistance by about two orders of magnitude compared to the ambient pressure value may suggest an insulator-to-metal transition with pressure. However, the temperature dependences of resistance $R(T)$ at various pressures, displayed in Fig. 5(b), show an insulating behavior up to the highest pressure of $\sim$55 GPa.

The resistance variations with temperature at various pressures were first plotted as $\ln R^{-1}$ vs T^{-1} and then as $\ln R^{-1}T$ vs T^{-1}. However, no significant straight-line region was observed in these graphs. We show in Fig. 5(c) plots of $\ln R$ vs $(T_0/T)^{1/4}$, these being indicative of the three-dimensional variable range hopping (3D VRH) law [45,46] where T_0 is the Mott temperature [47]. The resistance plots cover the pressure range 1.5–53 GPa. Their general behavior changes
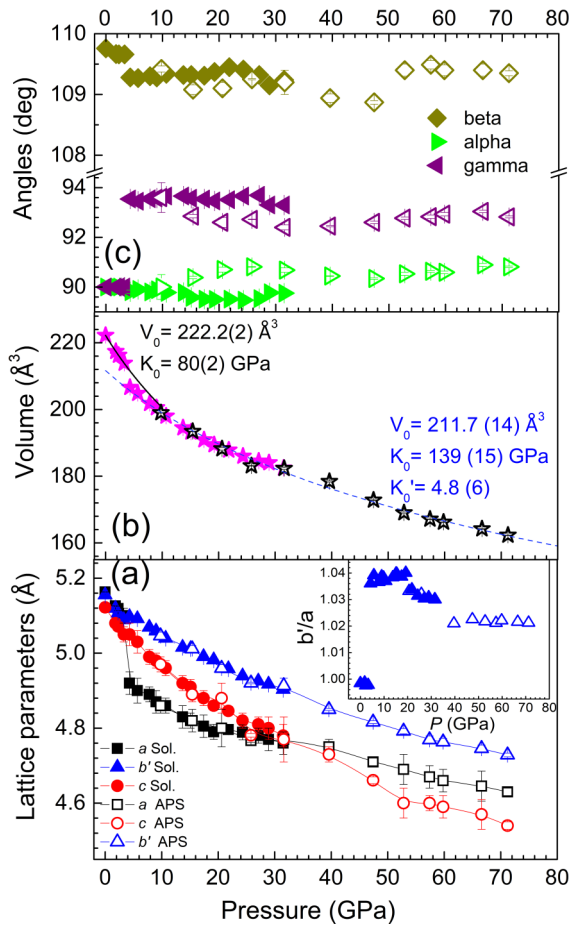
FIG. 3. Pressure dependence of the lattice parameters a, $b' = b/\sqrt{3}$, c (a), the unit-cell volume V (b), and angles α, β, and γ (c) of Li_2IrO_3. The solid and dashed lines in (b) are fits with second- and third-order Birch-Murnaghan equations of state, respectively (see text). Solid and open symbols correspond with Soleil and APS experiments, respectively. Note changes at the range 20–40 GPa in the behavior of lattice parameters and some volume deviation from the EOS calculated at the pressure range 4–72 GPa. In accord with this, the b'/a ratio [inset panel (a)] shows an appreciable decrease at the 20–40-GPa range.

significantly between 7 and 15 GPa and then between 34 and 43 GPa, however, almost does not change at the range 1.5–7 GPa, namely at the transition from the monoclinic $C2/m$ to the triclinic P-1 phase. The main features of the electrical conductivity variation as a function of pressure are the following:

Up to 7 GPa the resistance data fairly accurately obey the relation of $\ln R = \ln R_0 + (T_0/T)^{1/4}$ within the whole studied temperature range (300–75 K). However, above 15 GPa one can distinguish three temperature ranges (1)–(3) characterized by a different slope of the straight lines diminishing with temperature decrease [48]. A borderline between the first and second range shifts with pressure from ~140 to ~75 K, while the one between the second and third ranges remains at ~30 K.

At $P\sim43$ GPa $R(T)$ behavior changes drastically [Figs. 5(b) and 5(c)]; afterwards it stabilizes at least up to 55 GPa. It is noteworthy that the Mott temperature drops with pressure before becoming weakly P dependent above ~23 GPa [Fig. 5(d)].
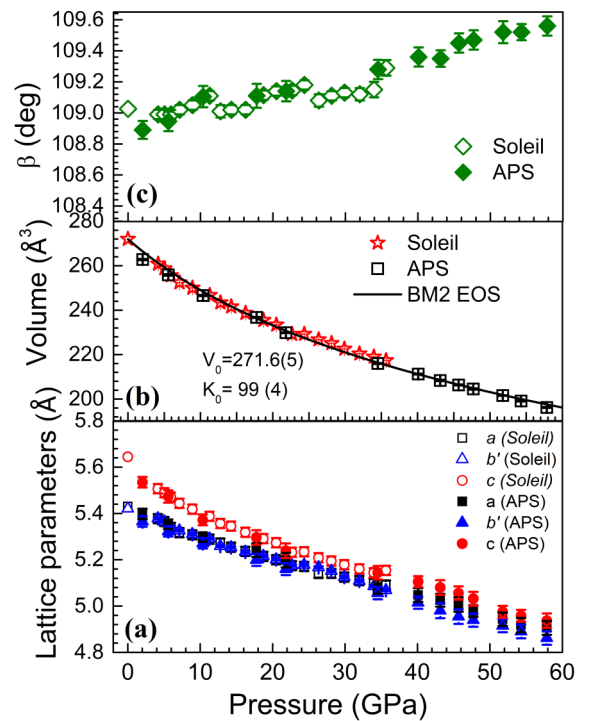

FIG. 4. Lattice parameters a, $b' = b/\sqrt{3}$, c (a), unit-cell volume V (b), and β (c) of Na_2IrO_3 as a function of external pressure. The volume V is fitted by the second-order Birch-Murnaghan equation of state as discussed in the text.

2. Na_2IrO_3

Resistance R as function of pressure up to about 80 GPa measured for Na_2IrO_3 at $T = 300$ K is plotted in Fig. 6(a). The measurement procedure was similar to the Li_2IrO_3 case. R decreases steadily with increasing pressure up to about 10 GPa after which a steeper decrease in R is found, followed by a gradual flattening above 35 GPa with the overall resistance decreasing by about two orders of magnitude from ambient pressure to ~45 GPa. This behavior is similar to what was recently observed for in-plane resistance measured for single-crystal Na_2IrO_3 up to 38 GPa [49] with some pressure delay. The latter implies that also in our case in-plane resistance tunes electrical transport properties of the sample. Above 45 GPa the resistance hardly changes with pressure and around 50 GPa there is the change of the sign of the dR/dP derivative and a continuous slight increase in R. During the decompression cycle, we found that the resistance retraces the compression data down to about 45 GPa. Below 45 GPa, however, the resistance behavior shows some hysteresis: resistance almost does not change down to ~30 GPa and only then slowly increases with pressure decrease. The ambient pressure value of R, obtained after the decompression cycle, is about 30 times smaller compared to the initial ambient pressure value. This big difference can be explained due to compacting of the powder sample during the compression cycle.

Figure 6(b) shows the temperature dependent $R(T)$ at various pressures. Consistent with the $R(P)$ data shown in Fig. 6(a), the R drops rapidly with pressure until about 40 GPa, after which the $R(T)$ data for higher P almost overlap. All $R(T)$ data display, within the studied temperature range, a
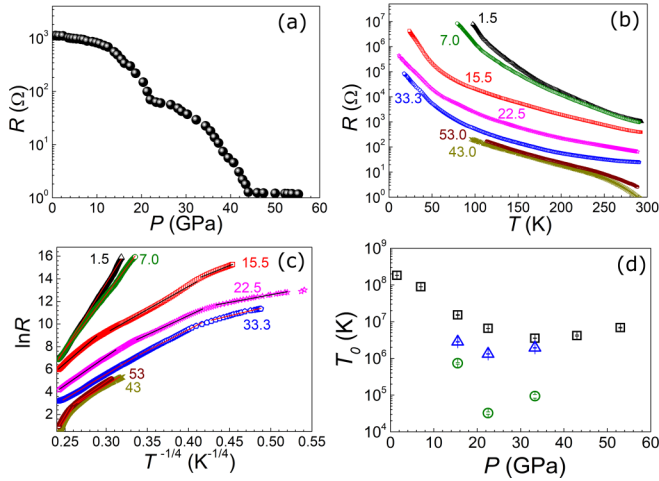
FIG. 5. (a) Pressure dependence of the resistance at 300 K for Li_2IrO_3. (b) Temperature dependence of the resistance measured at various pressures. (c) Linearized temperature-dependent data at various pressures assuming variable range hopping mechanism, $\ln R$ vs $(T_0/T)^{1/4}$. The Mott temperature T_0 is obtained from the slope of linear fits to these plots. Panel (d) shows the pressure dependence of T_0 for different characteristic temperature ranges: (1) 295 to 120 K; (2) 80 to 30 K; (3) below 30 K, designated as squares, triangles, and circles, respectively. Above 43 GPa the temperature range (1) is split into two ranges around 220 K. We present T_0 data for the range below 220 K; above ~220 K T_0 is about 2.1×10^8 K, similar to the value obtained at 1.5 GPa.

temperature dependence consistent with insulating behavior up to the highest pressures measured. These data rule out any metallic state at pressures up to 80 GPa for Na_2IrO_3. Figure 6(c) also shows plots of the data in terms of Arrhenius thermally activated hopping behavior. At all pressures at the studied temperature range, resistance data fairly well obey the Arrhenius behavior, $\ln(R) \propto E_a/k_B T + $ const, where k_B is the Boltzmann constant and E_a is the electrical transport activation energy. Figure 6(d) shows the pressure dependence of E_a obtained from the slope of fits to these plots, from whence the charge gap for intrinsic conduction $E_g = 2E_a$ is derived. The activation energy drops with pressure up to about 50 GPa after which it increases slowly again for higher P. We note that up to 38 GPa the obtained E_g values are in good agreement with the single-crystal in-plane data [49].

IV. DISCUSSION

Li_2IrO_3 undergoes the $C2/m \rightarrow P\text{-}1$ structural phase transition at the range of 3.5–7 GPa. This transition mainly affects the Ir hexagon network, leading to the formation of Ir-Ir dimers [23–25]. However, it hardly effects electrical transport properties, except a tiny ~4% resistance drop, and main changes are noticed only above ~14 GPa within the HP phase. In the case of Li_2IrO_3 the $R(T)$ data at various pressures are consistent with the Mott variable-range hopping law $\ln R = \ln R_0 + (T_0/T)^{1/4}$ [46,50] with the slope of the straight lines diminishing with increase of applied pressure; $k_B T_0$ values extracted from those data range from 1.5×10^4 eV at 1.5 GPa to 300 eV for $P = 33.2$ GPa.
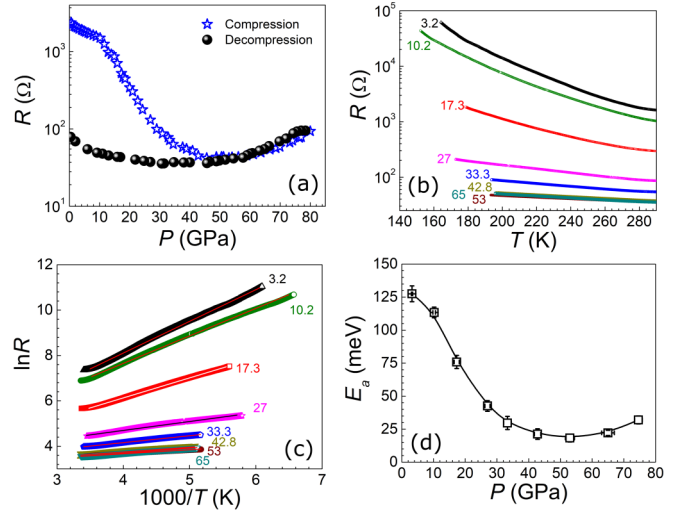

FIG. 6. (a) Pressure dependence of the resistance at 300 K for Na_2IrO_3. (b) Temperature dependence of the resistance measured at various pressures. (c) Linearized temperature-dependent data at various pressures assuming Arrhenius activated hopping transport, $\ln R \propto 1/T$. The activation energy E_a is obtained from the slope of linear fits to these plots to obtain the charge gap for intrinsic conduction $E_g = 2E_a$. Panel (d) shows the pressure dependence of E_a; the solid line through the data points is to guide the eye.

From T_0 values we can estimate a localization length α^{-1} using the relation [45]

$$\alpha^{-1} = [k_B T_0 N(E_F)/16]^{-1/3} \tag{1}$$

and the ratio of the localization length to the intersite distance a [51]:

$$(a\alpha)^{-1} \propto 5[k_B T_0 N*(E_F)]^{-1/3} \tag{2}$$

where $N(E_F)$ and $N*(E_F)$ are the density of states and the normalized density of states at the Fermi level. Assuming that $N*(E_F)$ is in the range of $1-10(\text{eV})^{-1}$ (see for example [52]) we will get the value 0.1–0.2 of $(a\alpha)^{-1}$ at 1.5 GPa which does not seem to be indicative of a simple variable-range hopping process. At $P = 33.2$ GPa, $(a\alpha)^{-1} \sim 0.35$–0.7 corresponding to a more significant overlap of the original localized wave functions under compression which is more realistic for a real $T^{1/4}$ behavior. We can propose that above ~14 GPa weakening of electron localization begins, resulting in the appreciable decrease of the resistance, about three orders of magnitude, at the range 14–44 GPa [Fig. 5(a)].

We note also a corroborating change of the a lattice parameter behavior above 20 GPa and some deviation of the unit-cell volume $V(P)$ dependence from the calculated EOS between 30 and 40 GPa [Figs. 3(b) and 3(c)]. The pressure evolution of the a axis observed between 20 and ~40 GPa leads to the convergence of the a and b parameters indicating reduction of the distortion of the Ir honeycomb lattice, which appeared as the result of Ir-Ir dimerization around 4 GPa. This suggests a possible reduction of the dimerization effect and some redistribution of the electron density in the Ir_6 hexagon [53]. This suggestion agrees well with the above-mentioned weakening of electron localization at the range 14–44 GPa. Around 44 GPa the $R(P)$ behavior drastically

changes: resistance hardly changes above this pressure and the Mott temperature shows a slight increase. This $R(P)$ feature corroborates with the stabilization of the b'/a ratio signifying a stabilization of the Ir hexagon shape at least up to 72 GPa. Thus, an appreciable change of electronic properties corroborating with some structural rearrangement takes place at the range of about 20–40 GPa within the HP structure.

In the case of Na_2IrO_3, recent *ab initio* density functional theory calculations [24] predict a structural $C2/m \rightarrow$ P-1 phase transition, similar to Li_2IrO_3, accompanied by a collapse of the Ir magnetic moments and a dimerization of the previously equally long Ir-Ir bonds in the *ab* plane, at about 45 GPa [24]. Furthermore, Hu *et al.* [54] suggest a sequence of successive structural and magnetic phase transitions, $C2/m \rightarrow P2_1/m \rightarrow P$-1 $\rightarrow P2_1/m$, at about 42, 47, and 55 GPa, respectively, distinguished by Ir-Ir bond ordering features. We note also that the crystal volume and lattice parameters in the *ab* plane of α-Li_2IrO_3 ($C2/m$) preceding the transition to the P-1 structure are consistent with the crystal volume and corresponding lattice parameters of Na_2IrO_3 extrapolated from the EOS to ~42 GPa. This estimation suggests a similar transition also in Na_2IrO_3 in good agreement with the above theoretical predictions. However, the performed XRD analysis does not confirm this suggestion: we can rule out the phase transitions predicted in previous studies [24,54] at least up to 58 GPa, as such a symmetry lowering would induce the appearance of additional peaks not observed in our study. Nevertheless, resistance studies show a drastic change of electrical transport features around 45 GPa resembling Li_2IrO_3, namely stabilization of the resistance at this pressure range. R vs P dependence flattens and furthermore changes the slope sign upon compression, with some hysteresis upon decompression. Our $R(P,T)$ data show that above 45 GPa Na_2IrO_3 remains a narrow-gap semiconductor with the electrical transport activation energy $E_a \sim 20$ meV which increases slightly with pressure up to the highest pressure measured, $P = 80$ GPa (the charge gap for intrinsic conduction $E_g = 2E_a \sim 40$ meV).

We note an unexpected concurrence of the electrical transport behavior for Li and Na irridates at pressures above ~45 GPa. Indeed, despite many dissimilarities, namely different conductivity mechanism and different structural features, the resilient nonmetallic behavior makes both systems very similar. Importantly, in both irridates the observed significant change of electronic properties around 45 GPa and the onset of an unusual electronic state does not correspond with a structural phase transition. This distinguishes the studied systems from Sr_2IrO_4 [33], where a similar electronic state appears as the result of a structural phase transition. Furthermore, the obtained results suggest that within a very broad pressure range the behavior of the studied irridates lies in between the fully itinerant and the fully localized description. Recently Streltsov and Khomskii [34] proposed a possibility of the appearance of particular states close to a localized-itinerant crossover, so that the Mott transition occurs stepwise. First, the electrons are delocalized in finite clusters, forming "molecules" in a solid—the hopping between such molecules being still small enough to render the whole system insulating, but with electrons localized rather on such "molecular clusters" and not on isolated sites. Only later, at still much higher

pressures, can one reach a state of a homogeneous metal in which electrons would really be itinerant, delocalized over the whole system. Particularly, in the case of iridates, where IrO_6 octahedra form a honeycomb lattice sharing their edges, if one includes hopping via ligand p orbitals, then the d electron can hop only within one particular hexagon and cannot move to another one [5,55]. Thus, the nature of electrons in this case is twofold: they are completely delocalized over the corresponding six Ir sites, but localized on a particular Ir_6 hexagon on some extended quasimolecular orbitals (QMOs) [56], thus making the compound both strongly localized and highly itinerant.

It is noteworthy that the nature of such molecular clusters is governed by the type of electron hopping: d-d or p-d. The p-d hopping via the ligand p orbitals may result in the formation of QMOs living on hexagons, where the d electron can hop only within one particular hexagon and cannot move to another one, while the direct d-d hopping would favor a strong metal-metal bond on particular two-site bonds [34]. It could be proposed that in α-Li_2IrO_3, characterized by smaller metal-metal distances and dimer formation, direct d-d hopping may dominate or start to be dominating at high pressure, while in Na_2IrO_3 p-d hopping may play a more significant role. The observed weakening of the electron localization coinciding with the convergence of the a and b parameters preceding the onset of the unusual electronic state in Li_2IrO_3 agree well with the discussed model of QMOs living on two-site bonds. While in Na_2IrO_3 in the absence of a dimerization transition, the Ir-hexagon looks as a preferable molecular cluster. However, undoubtedly a further thorough, preferably single-crystal, XRD study is necessary for a more clear understanding of the nature of this unusual electronic state arising in iridates at high pressures.

V. CONCLUSIONS

Our studies reveal rather different behavior of Li_2IrO_3 and Na_2IrO_3 under pressure. While Li_2IrO_3 undergoes a structural transition from a slightly distorted monoclinic $C2/m$ phase to the highly distorted dimerized triclinic P-1 phase at ~4 GPa, in Na_2IrO_3 despite some theoretical predictions [24,46] a similar transition does not occur at least up to 57 GPa. Moreover, these materials reveal different mechanisms of the electrical conductivity: Na_2IrO_3 is characterized by Arrhenius conductivity within the entire pressure range (up to 65 GPa), while in Li_2IrO_3 conductivity is consistent with the Mott variable-range hopping law. With that, the conductivity features of Li_2IrO_3 change significantly around 20 GPa, corroborating with the appreciable change of the a-lattice parameter behavior suggesting a change of the structural and electrical transport features. Notwithstanding the above-mentioned appreciable differences, at pressures around 45 GPa both studied iridates demonstrate rather similar features: namely, an onset of an unusual electronic state not accompanied by (or resulting from) a structural phase transition, which despite a preceding significant unit-cell volume densification is characterized by the resilient nonmetallic behavior. Thus, Na_2IrO_3 demonstrates a rather small and stable energy gap (~40 meV above ~40 GPa) and even a clear trend to a slight resistance increase, a so-called "U-shaped" curve. This resilient nonmetallic

behavior of the iridates, observed recently also in Sr_2IrO_4 and $Sr_3Ir_2O_7$ [31,33], looks rather universal and is of great interest and undoubtedly needs additional structural, preferably single-crystal XRD, studies in order to further clarify the nature of the HP insulating state. It could be proposed that this behavior is due to the formation of particular states close to a localized-itinerant crossover, characterized by electrons, delocalized in finite clusters, forming "molecules" in a solid, but still localized on such molecular clusters [5,34]. Formation of such states suggests in the present case a "partial," stepwise Mott transition, which only at higher pressures will be completed by a general electron delocalization and formation of a homogeneous metal. We note that these unusual states emerge in the studied iridates independently from the buffer element at almost the same pressure ($\sim$45 GPa). This similarity is surprising, given that these materials are characterized by rather different Ir-O and Ir-Ir interatomic distances, and an understanding of this finding seems essential for understanding the nature of conductivity in iridates.

ACKNOWLEDGMENTS

[1] G. Jackeli and G. Khaliullin, Phys. Rev. Lett. **102**, 017205 (2009).

[2] J. Chaloupka, G. Jackeli, and G. Khaliullin, Phys. Rev. Lett. **105**, 027204 (2010).

[3] J. Chaloupka, G. Jackeli, and G. Khaliullin, Phys. Rev. Lett. **110**, 097204 (2013).

[4] H. Gretarsson, J. P. Clancy, Y. Singh, P. Gegenwart, J. P. Hill, J. Kim, M. H. Upton, A. H. Said, D. Casa, T. Gog, and Y.-J. Kim, Phys. Rev. B **87**, 220407(R) (2013).

[5] K. Foyevtsova, H. O. Jeschke, I. I. Mazin, D. I. Khomskii, and R. Valentí, Phys. Rev. B **88**, 035107 (2013).

[6] V. M. Katukuri, S. Nishimoto, V. Yushankhai, A. Stoyanova, H. Kandpal, S. Choi, R. Coldea, I. Rousochatzakis, L. Hozoi, and J. van den Brink, New J. Phys. **16**, 013056 (2014).

[7] Y. Yamaji, Y. Nomura, M. Kurita, R. Arita, and M. Imada, Phys. Rev. Lett. **113**, 107201 (2014).

[8] N. B. Perkins, Y. Sizyuk, and P. Wölfle, Phys. Rev. B **89**, 035143 (2014).

[9] S. Hwan Chun, J.-W. Kim, J. Kim, H. Zheng, C. C. Stoumpos, C. D. Malliakas, J. F. Mitchell, K. Mehlawat, Y. Singh, Y. Choi, T. Gog, A. Al-Zein, M. M. Sala, M. Krisch, J. Chaloupka, G. Jackeli, G. Khaliullin, and B. J. Kim, Nat. Phys. **11**, 462 (2015).

[10] Y. Singh and P. Gegenwart, Phys. Rev. B **82**, 064412 (2010).

[11] X. Liu, T. Berlijn, W.-G. Yin, W. Ku, A. Tsvelik, Y.-J. Kim, H. Gretarsson, Y. Singh, P. Gegenwart, and J. P. Hill, Phys. Rev. B **83**, 220403(R) (2011).

[12] I. Kimchi and Y.-Z. You, Phys. Rev. B **84**, 180407(R) (2011).

[13] S. K. Choi, R. Coldea, A. N. Kolmogorov, T. Lancaster, I. I. Mazin, S. J. Blundell, P. G. Radaelli, Y. Singh, P. Gegenwart, K. R. Choi, S.-W. Cheong, P. J. Baker, C. Stock, and J. Taylor, Phys. Rev. Lett. **108**, 127204 (2012).

[14] F. Ye, S. Chi, H. Cao, B. C. Chakoumakos, J. A. Fernandez-Baca, R. Custelcean, T. F. Qi, O. B. Korneta, and G. Cao, Phys. Rev. B **85**, 180403(R) (2012).

[15] Y. Singh, S. Manni, J. Reuther, T. Berlijn, R. Thomale, W. Ku, S. Trebst, and P. Gegenwart, Phys. Rev. Lett. **108**, 127203 (2012).

[16] H. Gretarsson, J. P. Clancy, X. Liu, J. P. Hill, E. Bozin, Y. Singh, S. Manni, P. Gegenwart, J. Kim, A. H. Said, D. Casa, T. Gog, M. H. Upton, H.-S. Kim, J. Yu, V. M. Katukuri, L. Hozoi, J. van den Brink, and Y.-J. Kim, Phys. Rev. Lett. **110**, 076402 (2013).

[17] R. Comin, G. Levy, B. Ludbrook, Z.-H. Zhu, C. N. Veenstra, J. A. Rosen, Y. Singh, P. Gegenwart, D. Stricker, J. N. Hancock, D. van der Marel, I. S. Elfimov, and A. Damascelli, Phys. Rev. Lett. **109**, 266406 (2012).

[18] S. M. Winter, A. A. Tsirlin, M. Daghofer, J. van den Brink, Y. Singh, P. Gegenwart, and R. Valentí, J. Phys.: Condens. Matter **29**, 493002 (2017).

[19] Y. Miura, M. Sato, Y. Yamakawa, T. Habaguchi, and Y. Ōno, J. Phys. Soc. Jpn. **78**, 094706 (2009).

[20] G. Jackeli and D. I. Khomskii, Phys. Rev. Lett. **100**, 147203 (2008).

[21] G. Bastien, G. Garbarino, R. Yadav, F. J. Martinez-Casado, R. Beltrán Rodríguez, Q. Stahl, M. Kusch, S. P. Limandri, R. Ray, P. Lampen-Kelley, D. G. Mandrus, S. E. Nagler, M. Roslova, A. Isaeva, T. Doert, L. Hozoi, A. U. B. Wolter, B. Büchner, J. Geck, and J. van den Brink, Phys. Rev. B **97**, 241108(R) (2018).

[22] T. Biesner, S. Biswas, W. Li, Y. Saito, A. Pustogow, M. Altmeyer, A. U. B. Wolter, B. Büchner, M. Roslova, T. Doert,

S. M. Winter, R. Valentí, and M. Dressel, Phys. Rev. B **97**, 220401(R) (2018).

[23] Y. Singh, S. Layek, K. Mehlawat, E. Greenberg, G. Kh. Rozenberg, and M. P. Pasternak, Bull. Am. Phys. Soc. **61**, L33.011 (2016).

[24] V. Hermann, M. Altmeyer, J. Ebad-Allah, F. Freund, A. Jesche, A. A. Tsirlin, M. Hanfland, P. Gegenwart, I. I. Mazin, D. I. Khomskii, R. Valentí, and C. A. Kuntscher, Phys. Rev. B **97**, 020104(R) (2018).

[25] J. P. Clancy, H. Gretarsson, J. A. Sears, Y. Singh, S. Desgreniers, K. Mehlawat, S. Layek, G. Kh. Rozenberg, Y. Ding, M. H. Upton, D. Casa, N. Chen, J. Im, Y. Lee, R. Yadav, L. Hozoi, D. Efremov, J. van den Brink, and Y.-J. Kim, npj Quantum Mater. **3**, 35 (2018).

[26] G. Cao and P. Schlottmann, Rep. Prog. Phys. **81**, 042502 (2018).

[27] B. J. Kim, H. Ohsumi, T. Komesu, S. Sakai, T. Morita, H. Takagi, and T. Arima, Science **323**, 1329 (2009).

[28] W. Witczak-Krempa, G. Chen, Y. B. Kim, and L. Balents, Annu. Rev. Condens. Matter Phys. **5**, 57 (2014).

[29] J. G. Rau, E. K.-H. Lee, and H.-Y. Kee, Annu. Rev. Condens. Matter Phys. **7**, 195 (2016).

[30] D. Pesin and L. Balents, Nat. Phys. **6**, 376 (2010).

[31] D. A. Zocco, J. J. Hamlin, B. D. White, B. J. Kim, J. R. Jeffries, S. T. Weir, Y. K. Vohra, J. W. Allen, and M. B. Maple, J. Phys.: Condens. Matter **26**, 255603 (2014).

[32] Y. Ding, L. Yang, C.-C. Chen, H.-S. Kim, M. J. Han, W. Luo, Z. Feng, M. Upton, D. Casa, J. Kim, T. Gog, Z. Zeng, G. Cao, H.-K. Mao, and M. van Veenendaal, Phys. Rev. Lett. **116**, 216402 (2016).

[33] C. Chen, Y. Zhou, X. Chen, T. Han, C. An, Y. Zhou, Y. Yuan, B. Zhang, S. Wang, R. Zhang, L. Zhang, C. Zhang, Z. Yang, L. E. DeLong, and G. Cao, Phys. Rev. B **101**, 144102 (2020).

[34] S. V Streltsov and D. I. Khomskii, Phys. Usp. **60**, 1121 (2017).

[35] G. Y. Machavariani, M. P. Pasternak, G. R. Hearne, and G. Kh. Rozenberg, Rev. Sci. Instrum. **69**, 1423 (1998).

[36] A. P. Hammersley, S. O. Svensson, M. Hanfland, A. N. Fitch, and D. Hausermann, High Press. Res. **14**, 235 (1996).

[37] A. P. Hammersley, ESRF Internal Report, ESRF97HA02T (ESRF, Grenoble, 1997).

[38] C. Prescher and V. B. Prakapenka, High Press. Res. **35**, 223 (2015).

[39] B. H. Toby and R. B. Von Dreele, J. Appl. Crystallogr. **46**, 544 (2013).

[40] G. S. Pawley, J. Appl. Crystallogr. **14**, 357 (1981).

[41] A. D. Chijioke, W. J. Nellis, A. Soldatov, and I. F. Silvera, J. Appl. Phys. **98**, 114905 (2005).

[42] Y. Akahama and H. Kawamura, J. Appl. Phys. **100**, 043516 (2006).

[43] F. Birch, J. Geophys. Res. **83**, 1257 (1978).

[44] V. Hermann, J. Ebad-Allah, F. Freund, I. M. Pietsch, A. Jesche, A. A. Tsirlin, J. Deisenhofer, M. Hanfland, P. Gegenwart, and C. A. Kuntscher, Phys. Rev. B **96**, 195137 (2017).

[45] I. G. Austin and N. F. Mott, Adv. Phys. **18**, 41 (1969).

[46] N. F. Mott, *Metal-Insulator Transitions* (Taylor & Francis, London, 1990).

[47] It is noteworthy that we have attempted also a two-dimentional VRH regime ($T^{-1/2}$) fitting. At low pressures ($P \leqslant 7$ GPa), where data can be fitted with the single fit parameters, a linear fit with $T^{-1/4}$ dependence (3D VRH) looks a bit better compared to the 2D VRH. Correspondingly, we chose the 3D option.

[48] We note that a similar $R(T)$ trend to a saturation at low temperatures was observed previously for some other system, e.g., Na_2IrO_3 [49], magnetite [51], etc.

[49] X. Xi, X. Bo, X. S. Xu, P. P. Kong, Z. Liu, X. G. Hong, C. Q. Jin, G. Cao, X. Wan, and G. L. Carr, Phys. Rev. B **98**, 125117 (2018).

[50] N. F. Mott, in *Festkörperproblem Advanced Solid State Physics*, edited by J. Treusch, Vol. XIX (Vieweg, Braunschweig, 1979), p. 331.

[51] G. Kh. Rozenberg, G. R. Hearne, M. P. Pasternak, P. A. Metcalf, and J. M. Honig, Phys. Rev. B **53**, 6482 (1996).

[52] V. A. M. Brabers, Phys. B: Condens. Matter **205**, 143 (1995).

[53] It is well known that Li_2IrO_3 samples are characterized usually by a significant number of different defects and we cannot exclude their influence on electrical transport properties and conductivity mechanism. However, only a defect structure cannot explain the observed correlation between the changes of electronic and structural properties above 20 GPa.

[54] K. Hu, Z. Zhou, Y.-W. Wei, C.-K. Li, and J. Feng, Phys. Rev. B **98**, 100103 (2018).

[55] S. Streltsov, I. I. Mazin, and K. Foyevtsova, Phys. Rev. B **92**, 134408 (2015).

[56] I. I. Mazin, H. O. Jeschke, K. Foyevtsova, R. Valentí, and D. I. Khomskii, Phys. Rev. Lett. **109**, 197201 (2012).